Hindawi
Journal of Nanomaterials
Volume 2018, Article ID 8612158, 14 pages
https://doi.org/10.1155/2018/8612158

Research Article

Biofabrication of Zinc Oxide Nanoparticle from *Ochradenus baccatus* Leaves: Broad-Spectrum Antibiofilm Activity, Protein Binding Studies, and *In Vivo* Toxicity and Stress Studies

Nasser A. Al-Shabib,[1] Fohad Mabood Husain,[1] Iftekhar Hassan,[2] Mohd Shahnawaz Khan,[3] Faheem Ahmed,[4] Faizan Abul Qais,[5] Mohammad Oves,[6] Mashihur Rahman,[7] Rais Ahmad Khan,[8] Altaf Khan,[9] Afzal Hussain,[10] Ibrahim M. Alhazza,[2] Shazia Aman,[11] Saba Noor,[12] Hossam Ebaid,[2] Jameel Al-Tamimi,[2] Javed Masood Khan,[1] Abdul Rehman M. Al-Ghadeer,[7] Md Khurshid Alam Khan,[7] and Iqbal Ahmad[5]

[1] *Department of Food Science and Nutrition, College of Food and Agriculture, King Saud University, Riyadh 11451, Saudi Arabia*
[2] *Department of Zoology, College of Science, King Saud University, Riyadh 11451, Saudi Arabia*
[3] *Protein Research Chair, Department of Biochemistry, College of Science, King Saud University, Riyadh 11451, Saudi Arabia*
[4] *College of Science & General Studies, Alfaisal University, Riyadh 11533, Saudi Arabia*
[5] *Department of Agricultural Microbiology, Aligarh Muslim University, Aligarh 202002, India*
[6] *Center of Excellence in Environmental Studies (CEES), King Abdulaziz University, Jeddah, Saudi Arabia*
[7] *School of Life Sciences, B. S. Abdur Rahman University, Vandalur, Chennai 600048, India*
[8] *Department of Chemistry, College of Science, King Saud University, Riyadh 11451, Saudi Arabia*
[9] *Central Laboratory Research Center, College of Pharmacy, King Saud University, Riyadh 11451, Saudi Arabia*
[10] *Department of Pharmacognosy, College of Pharmacy, King Saud University, Riyadh 11451, Saudi Arabia*
[11] *Department of Biochemistry, J. N. Medical College and Hospital, Aligarh Muslim University, Aligarh 202002, India*
[12] *Rajiv Gandhi Centre for Diabetes and Endocrinology, J. N. Medical College and Hospital, Aligarh Muslim University, Aligarh 202002, India*

Correspondence should be addressed to Nasser A. Al-Shabib; nalshabib@ksu.edu.sa and Fohad Mabood Husain; fhussain@ksu.edu.sa

Received 20 July 2017; Revised 15 November 2017; Accepted 5 December 2017; Published 7 February 2018

Academic Editor: Piersandro Pallavicini

Biofilms are complex aggregation of cells that are embedded in EPS matrix. These microcolonies are highly resistant to drugs and are associated with various diseases. Biofilms have greatly affected the food safety by causing severe losses due to food contamination and spoilage. Therefore, novel antibiofilm agents are needed. This study investigates the antibiofilm and protein binding activity of zinc nanoparticles (ZnNPs) synthesized from leaf extract of *Ochradenus baccatus*. Standard physical techniques, including UV-visible spectroscopy Fourier transform infrared spectroscopy and X-ray diffraction and transmission electron microscopy, were used to characterize the synthesized OB-ZnNPs. Synthesized OB-ZnNPs demonstrated significant biofilm inhibition in human and food-borne pathogens (*Chromobacterium violaceum*, *Escherichia coli*, *P. aeruginosa*, *Klebsiella pneumoniae*, *Serratia marcescens*, and *Listeria monocytogenes*) at subinhibitory concentrations. OB-ZnNPs significantly reduced the virulence factors like violacein, prodigiosin, and alginate and impaired swarming migration and EPS production. OB-ZnNPs demonstrated efficient binding with HSA protein and no change in their structure or stability was observed. In addition, *in vivo* toxicity evaluation confirmed that OB-ZnNPs possessed no serious toxic effect even at higher doses. Moreover, they were found to have excellent antioxidant properties that can be employed in the fields of food safety and medicine. Hence, it is envisaged that the OB-ZnNPs can be used as potential nanomaterials to combat drug resistant bacterial infections and prevent contamination/spoilage of food.

1. Introduction

Biofilms are a complex aggregation of bacteria that colonize and are found embedded, in self-secreted exopolysaccharide (EPS) matrix, which contains polysaccharides, proteins, lipids, and nucleic acids. Biofilms are more resistant to antibiotics as compared to their planktonic forms [1]. Apart from making the inhabitants more resistant, biofilms also increase retention of water and nutrients and absorption of nutrients, protect against host immune responses, and facilitate horizontal gene transfer. Biofilm inhabitants demonstrate multicellular behavior similar to higher multicellular organisms [2]. Implications of biofilm formation in medical field are well known, as it is associated with various diseases, infections caused by medical devices and nosocomial infections [3, 4]. Biofilms have also become problematic in the food industries, including brewing [5], seafood processing [6], dairy processing [7], poultry processing [8], and meat processing [9] leading to food safety issues by causing spoilage and contamination of food and food contact materials. There is an urgent need to find nontoxic, stable antibiofilm agents to improve public health and minimize economic losses.

Advent of nanotechnology has made nanomaterials as an effective alternative antimicrobial strategy to treat drug-resistant infections [10]. Particles with less than 100 nm in size are termed as nanoparticles (NPs) and their potent biocidal properties are attributed to their small size and high surface-to-volume ratio [11, 12]. In addition, stability of metal and metal oxides than organic compounds make them better antimicrobial agents [13, 14]. Among metal oxides, ZnO has attracted attention as antibacterial agent and ZnO nanoparticles (ZnO-NPs) are known to exhibit broad-spectrum antibacterial activity and can reduce the attachment and viability of microbes [15, 16]. Further, it is well established that the nanoparticles, after entry into the host system interact with biomolecules like proteins, lipids, and nucleic acids. Therefore, the effects of NPs are combined actions of nanoparticle-protein "corona" rather than nanoparticle alone [17]. Therefore, understanding of protein NPs interaction is very important for its future applications in medical and food industry [18, 19] However, minimal work has been carried out to synthesize nontoxic ZnO nanoparticles and study their interactions with proteins and effects on biofilm formed by human and foodborne pathogens.

Green synthesis of NPs using plants is preferred over other chemical and physical methods as it is cost-effective, ecofriendly, and safe for human therapeutic use [20] and can be utilized for large-scale NPs synthesis [21]. ZnO nanoparticles (ZnONPs) from plants have been synthesized using green chemistry approaches by several workers [22–24].

Ochradenus baccatus Del. belongs to family Resedaceae and is widely distributed in South-West and central regions of Saudi Arabia. *O. baccatus* (Del.) is a shrub and is very important medicinally as it contains high contents of antioxidants and anti-inflammatory agents [25]. Leaves of *Ochradenus baccatus* have been used in the treatment of microbial infections, diphtheria, ganglions, and allergies [26].

In this study, aqueous leaf extract of *Ochradenus baccatus* was used as reducing, capping, and stabilizing agent for the formation of zinc oxide nanoparticles (OB-ZnNPs). These nanoparticles were investigated for their ability to inhibit biofilm formed by bacterial pathogens. We also assessed its effect on the production of virulence factors like exopolysaccharide production, and motility associated with biofilm formation in the test pathogens. Further, the biofabricated OBZnNPs were examined for their protein (HSA) binding and toxicity studies were also performed *in vivo*. In our knowledge, this is probably the first report on the synthesis of nontoxic zinc oxide nanoparticles from the leaves of *Ochradenus baccatus* and characterization of their antibiofilm and protein binding properties.

2. Material Methods

2.1. Bacterial Strains. The bacterial strains used in this study included *Chromobacterium violaceum* ATCC 12472, *Escherichia coli* ATCC 25922, *P. aeruginosa* PAO1, *Klebsiella pneumoniae* ATCC 700603, *Serratia marcescens* ATCC 13880, and *Listeria monocytogenes* (laboratory strain). All bacterial strains were cultivated on Luria-Bertani (LB) medium and maintained at 37°C, except *C. violaceum* and *S. marcescens*, for which the temperature was 30°C.

2.2. Preparation of Ochradenus baccatus (OB) Seed Extract. *Ochradenus baccatus* leaves were collected and washed several times with distilled water to remove the dust particles and then sun-dried to remove the residual moisture. Leaf extract was prepared by crushing leaves in a grinder and the resultant powder (10 g) was homogenized completely in 50 ml double-distilled water and incubated with constant stirring (100 rpm) at 80°C for 20 min. The resultant mixture was then filtered using Whatman filter papers No. 1 to remove debris. This extract was used for generating green zinc nanoparticles.

2.3. Zinc Nanoparticle Synthesis. All the reagents involved in the experiments were of analytical grade purity and utilized as received without further purification. Zinc nitrate (99.999%) was purchased from Sigma-Aldrich. The synthesis was carried out in a domestic microwave oven (Samsung, 750 W). We followed the method described by Al-Shabib et al. (2016); briefly, 0.05 M aqueous solution of zinc nitrate in 100 ml distilled water was prepared in which 10 ml *O. baccatus* leaf extract was added to obtain a mixture solution in a round-bottom flask and then put into a domestic microwave oven. Microwave irradiation proceeded at 100% power for 20 min. After microwave processing, the solution was cooled to room temperature. The resulting precipitate was separated by centrifugation, then washed with deionized water and absolute ethanol several times, and dried in an oven at 80°C for 24 h. Finally, the product was calcined at 800°C for 2 h [24].

2.4. UV-Visible Spectroscopy. The UV-visible spectral analysis was performed by using UV-Vis spectrophotometer (UV5704S from Electronics, India Ltd.) for surface plasmon resonance. The absorbance spectra was recorded in the range of 250–800 nm at room temperature in 1 cm path length

quartz cuvettes. Double distilled water was used as reference to correct the background absorption.

2.5. X-Ray Diffraction. The XRD of synthesized OB-ZnNPs nanoparticles were obtained using MiniFlex II benchtop XRD system (Rigaku Corporation, Tokyo, Japan). The diffraction pattern was acquired by CuKα radiation ($k = 1.54$ Å) at 30 mA current and operating at 40 kV. The angle of direction (2θ) data was recorded in the range of 20°–80°. Average crystalline size was calculated by Debye-Scherrer's equation:

$$D = \frac{K\lambda}{\beta \cos\theta}, \quad (1)$$

where D is average crystal size of nanoparticle, β is full width at half maximum of the diffraction peak, λ is wavelength of X-ray source used (1.54060 Å), and K is constant of Debye-Scherer equation with value ranging from 0.9 to 1.0 [27].

2.6. Fourier Transform Infrared Spectroscopy (FTIR). The transmittance spectra recorded by placing the dried powder of ZnO nanoparticles to spectroscopic grade KBr (mass ratio of about 1 : 100). FTR analysis was performed on Perkin Elmer FT-IR spectrometer Spectrum Two (Perkin Elmer Life and Analytical Sciences, CT, USA) at 4 cm^{-1} resolutions in diffuse reflectance mode in KBr pellets.

2.7. Scanning Electron Microscopy and EDX. Scanning electron micrographs of ZnO nanoparticles were obtained using JSM 6510LV scanning electron microscope (JEOL, Tokyo, Japan) equipped with Oxford Instruments INCAx-sight EDAX spectrometer to carry out analysis of constituting elements. The electron beams were accelerated at 15 kV. Images were obtained at 2500–35000x magnification.

2.8. Transmission Electron Microscopy (TEM). Transmission electron microscopy was done using EOL 100/120 kV TEM (JEOL, Tokyo, Japan). Aqueous suspension of ZnO nanoparticles was made in double distilled water followed by sonication at 30% amplitude for 15 min. About 10 μl of the suspension was transferred to TEM grid for analysis and excess amount of suspension was removed by soft filter paper. The grid was then allowed to dry at 80° for 6 h. Imaging was done at 200 kV in the magnification range of 300000–100000x magnification.

2.9. Determination of Minimal Inhibitory Concentration (MIC) of OB-ZnNPs. The MIC of OB-ZnNPs against each test pathogen was determined by the method of Clinical and Laboratory Standards Institute, USA with some modifications [28].

2.10. Violacein Inhibition Assay. Violacein production by *C. violaceum* (CV12472) in presence of OB-ZnNPs was studied using method of Blosser and Gray [29]. Briefly, CV12472 culture in the absence and presence of sub-MICs of OB-ZnNPs was grown overnight. 1 ml culture from each flask was centrifuged at 13000 ×g for 10 min and the pellet was dissolved in 1 ml DMSO. The solution was vortexed vigorously for 30 seconds to completely solubilize violacein and again centrifuged. Absorbance of the soluble violacein was read at 585 nm using microplate reader (Thermo Scientific, Multiskan Ex, India). Reduction in violacein production in the presence of mango extracts was measured in terms of % inhibition as [(OD of control − OD of treated)/OD of control] × 100.

2.11. Alginate Inhibition in PAO1. Overnight culture of *P. aeruginosa* (1%) was added to Luria-Bertani broth medium supplemented with or without OB-ZnNPs (25–200 μg/ml) and incubated overnight at 37°C under shaking. After incubation alginate production was estimated as described by Gopu et al. [30]. Briefly, 70 μl of test sample was mixed with 600 μl of boric acid-sulphuric acid solution (4 : 1) in an ice bath. The mixture was vortexed for 10 seconds and placed back again in ice bath. 20 μl of 0.2% carbazole dissolved in ethanol was added to the above mixture and vortexed for 10 s. The mixture was incubated for 30 min at 55°C and quantification was done at 530 nm using a microplate reader.

2.12. Prodigiosin Inhibition in S. marcescens. Prodigiosin production in *S. marcescens* was assayed using the method of Morohoshi et al. [31]. Briefly, 1% of *S. marcescens* cells (0.4 OD at 600 nm) were inoculated into 2 ml of fresh LB medium and incubated with and without sub-MICs of OB-ZnNPs (25–100 μg/ml). Late stationary phase cultures were collected and centrifuged at 10,000 rpm for 10 min. Prodigiosin from the cell pellet was extracted with acidified ethanol solution (4% 1 M HCl in ethanol) and absorbance was read at 534 nm using a UV-visible spectrophotometer.

2.13. Swarming Motility Assay. Swarming motility of the test pathogens was determined by the method of Husain and Ahmad [32]. Briefly, overnight cultures of test pathogens were point inoculated at the center of the 0.5% Luria-Bertani agar medium with or without sub-MICs of synthesized OB-ZnNPs.

2.14. Extraction and Quantification of Exopolysaccharide (EPS). Test pathogens (*P. aeruginosa*, *E. coli*, *L. monocytogenes*, *S. marcescens*, and *C. violaceum*) grown in the presence and absence of sub-MICs of OB-ZnNPs were centrifuged and supernatant was filtered. Three volumes of chilled ethanol (100%) were added to the resultant supernatant and incubated overnight at 4°C to precipitate EPS [33]. EPS was then quantified by measuring sugars following the method of Dubois et al. [34].

2.15. Assay for Biofilm Inhibition. Polyvinyl chloride microtiter plate assay was adopted to study the effect of OB-ZnNPs on biofilm formation of the test pathogens [35]. Briefly, overnight cultures of test pathogens were resuspended in fresh LB medium in the presence and the absence of OB-ZnNPs and incubated at 30°C for 24 h. The biofilms in the microtiter plates were stained with a crystal violet solution

and quantified by solubilizing the dye in ethanol and measuring the absorbance at OD_{470}.

2.16. Protein (HSA) Binding Studies with OB-ZnNPs

2.16.1. Binding of OB-ZnNPs to Human Serum Albumin: Tryptophan Fluorescence Analysis. Tryptophan fluorescence analysis of HSA in the absence and presence of NPs was measured according to previously mentioned procedure [36, 37] with minor modifications. Briefly, intrinsic fluorescence measurement of HSA (2 μM) was performed by titration with NPs (0-1 mg/ml) on a Jasco FP-750 fluorescence spectrophotometer at 25°C. The excitation wavelength was set as 295 nm and the emission spectra obtained were in the wavelength range of 300–400 nm. The excitation and emission slit widths were set as 5 nm. Respective blanks were subtracted; inner filter contribution was minimal and was less than 3%.

2.16.2. Stability of HSA in the Presence of NPs: Circular Dichroism Analysis. NPs induced secondary structural changes in HSA were measured by circular dichroism (CD) spectroscopy technique. Far UV-CD spectra of HSA (0.2 mg/ml) in the absence and presence of various concentrations of NPs (0.4 and 1 mg/ml) were recorded [38]. The samples were scanned from 200 to 250 nm three times, and the obtained data was averaged.

2.16.3. Nanoparticles-HSA Interaction: Hydrophobicity Measurement. 8-Anilinonaphthalene-1-sulfonic acid (ANS) is a frequently used extrinsic fluorophore having the propensity to interact with the exposed hydrophobic patches and is used for the determination of surface hydrophobicity in proteins. ANS fluorescence measurement of HSA (2 μM) incubated in the absence and presence of NPs (0-1 mg/ml) was performed on Jasco FP-750 spectrofluorometer. The excitation wavelength for ANS fluorescence measurements was set at 380 nm and emission spectra were recorded in the wavelength range of 400–600 nm. Both excitation and emission slits were set at 5 nm. Prior to measurements, aliquots were incubated at room temperature with 50-fold molar excess of ANS for 30 min in the dark [39].

2.17. Toxicity Studies

2.17.1. Animal Treatment Strategy. Twenty-four adult Swiss albino male adult mice (48–50 g, 6 months old) were bought from the central animal house, Department of Pharmacy, King Saud University, Riyadh, KSA. They were kept and treated under hygienic conditions maintained with 25 ± 5°C with 12 h day : night cycle as per the institutional guidelines. The animals were acclimatized for 10 days before beginning the treatment on standard pellet mice diet and fresh drinking water ad libitum. All the animals were randomly divided into four groups: control (normal without any treatment) named CN−, control positive (CN+), and CCl4 treated (single dose of 1 mL/kg in liquid paraffin in ratio of 1 : 1 by volume). The zinc nanoparticles were administered four times (once a week) at the dose of 2 mg/kg and 4 mg/kg of body weight denoted by OB-ZnNPs and OB-ZnNPs', respectively. All the doses were given by intraperitoneal mode using 1 ml insulin syringe. Carbon tetrachloride (CCl4), an established hepatotoxicant, was chosen as positive control for liver damage [40]. In the present study, dose and the duration of treatment were chosen to investigate if the nanoparticles induced any toxicity in the animals after repeated dose or not. After the treatment, all the animals were sacrificed on the same day under light ether anesthesia. Their livers and blood (with anticoagulant) were stored at −20°C until analysis.

2.17.2. Preparation of Samples. The serum was collected after centrifugation of blood samples at 1000 ×g for 10 min. The liver samples were homogenized separately at 3000 ×g in tris-HCl buffer (pH 7.36, 0.1 M) from which their supernatants were collected for biochemical assays and estimations.

2.17.3. Assay of Superoxide Dismutase (SOD) and Reduced Glutathione (GSH). The specific activity of SOD was assayed by autoxidation of pyrogallol in tris-succinate buffer by the method of S. Marklund and G. Marklund [41]. The level of GSH was estimated by method of Jollow et al. [42] based on DTNB reagent.

2.17.4. Estimation of Lipid Peroxidation. The lipid peroxidation was estimated by the method of Buege and Aust [43] involving the measurement of total malondialdehyde (MDA) based on reaction with TCA and TBA.

Estimation of SGOT and SGPT as Liver Function Markers. The activity of serum glutamate pyruvate transferase (SGPT) and serum glutamate oxaloacetate transferase (GOT) in the serum was assayed by commercially available estimation kits (Linear or QCA, Spain).

2.18. Statistical Analysis. All microbiological studies were performed in triplicate and the data obtained from experiments were presented, as mean values, and the difference between control and test was analysed using Student's *t*-test. All the data for the toxicity studies have been expressed as mean ± standard error of mean (SEM) for 6 different preparations in duplicate. Their statistical significance was evaluated by one-way ANOVA followed by Tuckey's method based software (Graph Pad prism 5). The treatment and the experiments were repeated twice to check the reproducibility of the results.

3. Results and Discussion

3.1. UV-Visible Spectral Analysis. The reducing ability of *Ochradenus baccatus* aqueous extract was evaluated for the synthesis of Zn nanoparticles. The UV-visible spectra of microwave assisted synthesis of ZnO nanoparticles are shown in Figure 1(a). The colour of reaction mixture, that is, 10 ml of *Ochradenus baccatus* aqueous extract and 100 ml of 0.05 mM zinc nitrate, was initially yellowish brown. When the reaction mixture was allowed for radiation in microwave for 20 min at 100% power, the colour of solution changed to off-white.

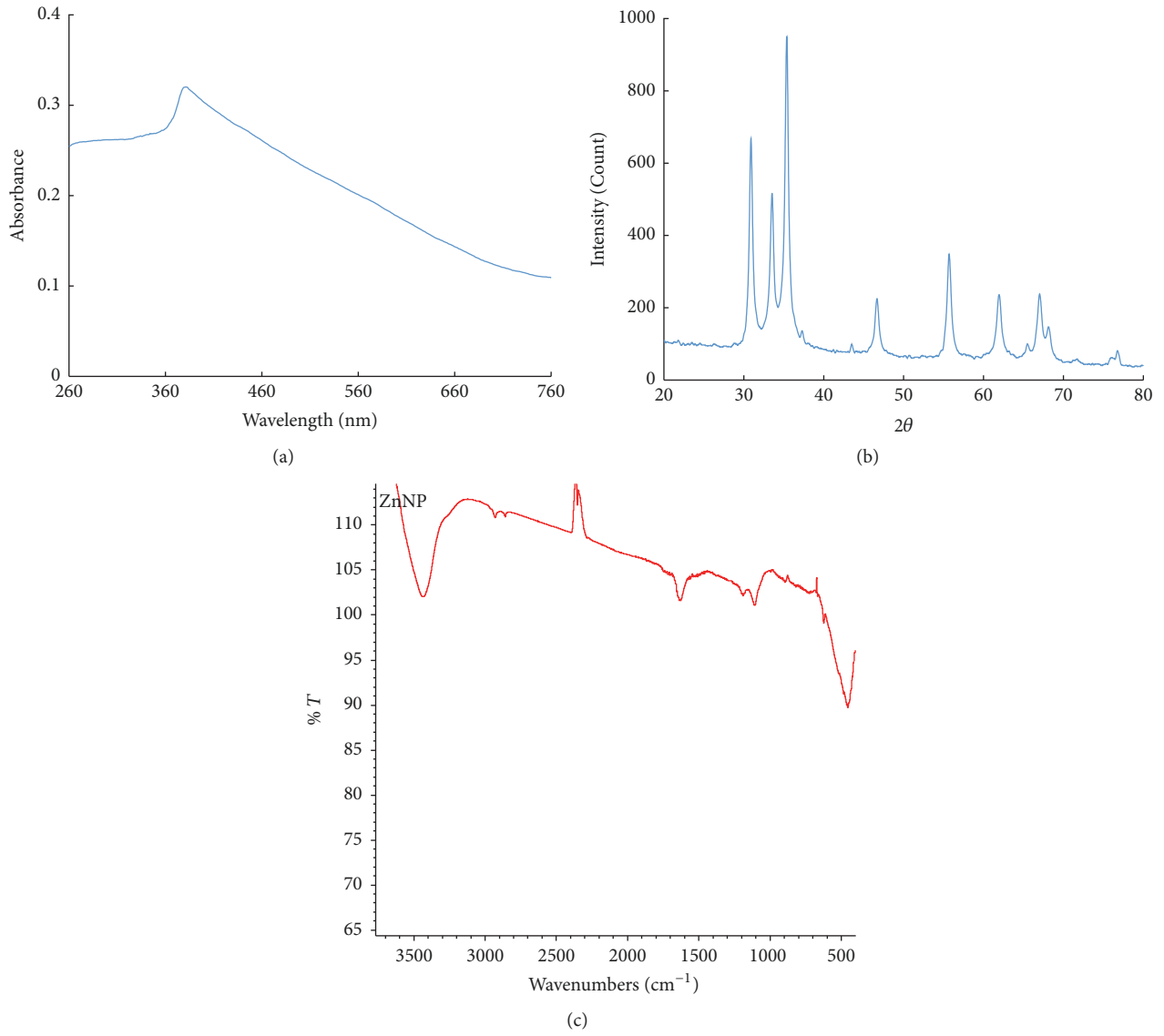

FIGURE 1: (a) UV-Vis absorption spectrum of ZnO nanoparticles *Ochradenus baccatus* leaf extract; (b) XRD patterns of ZnO nanoparticles using *Ochradenus baccatus* leaf extract; (c) FT-IR spectrum of synthesized ZnO nanoparticles.

Change in colour and absorption spectra with λ_{max} at 385 nm is considered as the preliminary characterization for synthesis of ZnO nanoparticles which is due to the reduction of Zn^{2+} ions. Similar result has been reported for synthesis of ZnO nanoparticles with characteristic peak around 372 nm [44]. ZnO nanoparticles synthesized for the leaf extract of *Aloe barbadensis* showed the absorption maxima in the range of 358–375, due to surface plasmon resonance [22].

3.2. X-Ray Diffraction. The XRD analysis was carried out for the determination of average article of ZnO nanoparticles. Figure 1(b) shows the XRD pattern of synthesized ZnO nanoparticles. XRD profile shows that the Bragg reflection was found to be prominent at 2θ values of 30.8°, 33.5°, and 35.3° with intensity of 668.4, 516.6, and 950.7. The full-width-at-half-maximum (FWHM) value at 35.3° was used for particle's size calculation. The average particle size was found to be 16.02 nm which was determined using Debye-Scherrer's equation.

3.3. Fourier Transform Infrared Spectroscopy (FTIR). FTIR analysis was carried out to evaluate the presence of various phytochemicals responsible for the synthesis as well as stabilization of ZnO nanoparticles (Figure 1(c)). The appearance of peak around 521 cm^{-1} is characteristic of hexagonal phase vibrations of ZnO nanoparticles [4]. Broad peak approximately at 3441 cm^{-1} is attributed to the vibrations of -OH group of phenols that might have acted as one of the capping agents of ZnO nanoparticles [5]. Another transmittance maxima around 1652 cm^{-1} were due to vibrations of primary amide of proteins. A short peak at 1085 cm^{-1} might be due to stretching of primary alcohols {R-CH_2-OH (1°)}. Thus, FTIR

Table 1: Minimum inhibitory concentrations (MICs) of OB-ZnNPs against test pathogens.

Strains	MIC of OB-ZnNPs (μg/ml)	Sub-MICs of OB-ZnNPs selected for assays (μg/ml)			
		1/16 × MIC	1/8 × MIC	1/4 × MIC	1/2 × MIC
P. aeruginosa	400	25	50	100	200
E. coli	50	3.125	6.25	12.5	25
C. violaceum	200	12.5	25	50	100
K. pneumoniae	200	12.5	25	50	100
S. marcescens	100	6.25	12.5	25	50
L. monocytogenes	100	6.25	12.5	25	50

analysis indicates that various phytoconstituents present in *Ochradenus baccatus* extract such as phenols, enzymes, proteins, and alcohols would have been responsible for synthesis and stabilization of ZnO nanoparticles. The capping of ZnO nanoparticles by these phytochemicals resulted in formation of protein corona that enhances its dispensability and ultimately lowers the agglomeration rate in aqueous medium. In addition to the above-mentioned phytocompounds, free amino and carboxylic groups have also been reported for their role in the stabilization of ZnO nanoparticles [22].

3.4. SEM and EDX Analysis. Scanning electron microscopy is one of the most routinely used techniques for the identification of shape of nanoparticles. Figures 2(a) and 2(b) show the scanning electron micrograph (SEM) of ZnO nanoparticles at 15000x and 35000x magnifications at 15 and 20 kV, respectively. It is evident from the surface scanning that the nanoparticles were predominantly found to be spherical and oval in shape. Although the particle size is not determined by SEM but it can be visualized that the nanoparticles are <100 nm. Figure 2(c) shows EDX pattern in which the highest elemental weight percent detected was of zinc with 62.0%. From Figure 2(d), oxygen, carbon, and sulphur were found to be 13.47, 23.37, and 1.16%, respectively. Nanoparticles with similar morphology from *Aloe barbadensis* [22] and *Nigella sativa* [24] have been reported.

3.5. Transmission Electron Microscopy. TEM images of ZnO nanoparticles are illustrated in Figure 2(e) at 30000x and 100000x magnification, respectively. The nanoparticle's micrograph shows that there was variation in shape and size of nanoparticles. The two-dimensional geometry of nanoparticles was found to be circular, elliptical, and somewhat hexagonal or irregular. The particles size is less than 50 nm and is consistent with the results of XRD.

3.6. Minimum Inhibitory Concentration. Minimum inhibitory concentrations (MIC) of OB-ZnNPs were assessed for all test pathogens and the results are summarized in Table 1. Concentrations below MIC, that is, sub-MICs, were considered for all assays.

3.7. Violacein Inhibition Assay in C. violaceum 12472. The result of the violacein assay is shown in Figure 3(a). The sub-MICs of OB-ZnNPs exhibited concentration-dependent inhibitory activity and all tested concentrations of OB-ZnNPs led to a statistically significant ($p \leq 0.05$) reduction in violacein production of *C. violaceum* compared to that of the untreated control. Our findings on violacein inhibition are in accordance with reports with silver nanowires [45] and zinc oxide nanostructures synthesized from the seed extract of *Nigella sativa* [24].

3.8. Inhibition of Alginate Production in P. aeruginosa PAO1. Alginate is a major constituent of the EPS of PAO1 biofilm; the effect of sub-MICs of OB-ZnNPs was studied for its efficacy to reduce the production of alginate. The obtained results showed that the alginate production was reduced significantly with increasing concentration of the synthesized zinc nanoparticles. At concentrations ranging 25–200 μg/ml, OB-ZnNPs inhibited alginate production by 34–74% in PAO1 (Figure 3(b)). The concentration-dependent inhibition of alginate by sub-MICs of OB-ZnNPs depicted in Figure 3(b) is an important finding as alginate confers resistance to the pathogens against antimicrobial agents. Inhibition of alginate production would reduce the rate of resistance among bacteria and make them susceptible to the drugs. Previously, mycofabricated biosilver nanoparticles have been shown to inhibit alginate production in *P. aeruginosa* [46].

3.9. Effect on Prodigiosin Production of S. marcescens. Dose-dependent decrease in the production of prodigiosin by *S. marcescens* was recorded at the sub-MICs ranging from 6.25–50 μg/ml. Though the inhibition was statistically insignificant at lower concentrations (6.25 and 12.5 μg/ml) but at higher concentrations, that is, 25 and 50 μg/ml significant ($p \leq 0.05$) reduction of 55 and 60%, respectively, was recorded (Figure 3(c)). Prodigiosin is considered as a major virulence factor of the *S. marcescens* and is quorum sensing regulated [31]. Hence, inhibition of prodigiosin will reduce the pathogenicity of *S. marcescens*. Prodigiosin inhibition is previously reported with natural products [47] and bacterial supernatant [48] but this is probably the first report on zinc nanoparticle impairing prodigiosin production in *S. marcescens*.

3.10. Biofilm Inhibition by OB-ZnNPs. In the present study, subinhibitory concentrations (1/16 × MIC-1/2 × MIC) of OB-ZnNPs were tested against biofilm formation of six human and foodborne bacterial pathogens, namely, *P. aeruginosa*

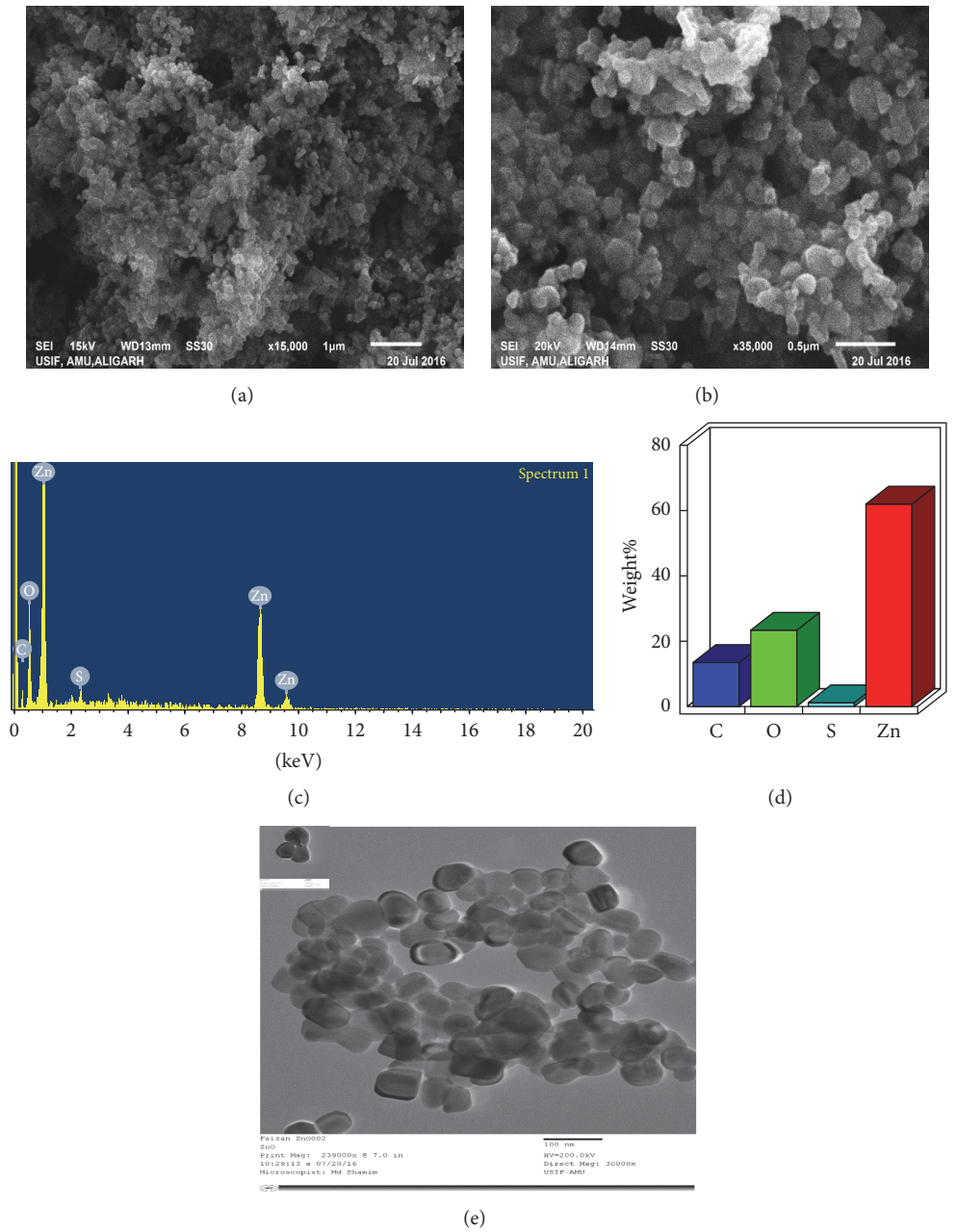

Figure 2: (a) and (b) show the SEM micrograph of ZnO nanoparticles at 15000x and 35000x magnifications, respectively; (c) and (d) show EDX pattern; (e) TEM micrograph of ZnO nanoparticles. Inset shows the corresponding HRTEM image of the synthesized nanoparticles.

PAO1, *E. coli* 25922, *L. monocytogenes*, *K. pneumonia*, *S. marcescens*, and *C. violaceum* 12472. Figure 4 shows the representative micrographs indicating that OB-ZnNPs inhibit biofilm formation in all the test pathogens in a dose-dependent manner. The data revealed 32, 52, 68, and 84% % inhibition of biofilm in *P. aeruginosa* PAO1; 18, 28, 49, and 67% in *E. coli* 25922; 28, 41, 63, and 78% in *L. monocytogenes*; 16, 30, 52, and 70% in *K. pneumoniae*; 39, 57, 69, and 80% in *S. marcescens*; and 24, 38, 54, and 64% in *C. violaceum* 12472, as compared to untreated control (Figure 4).

Formation of biofilm not only plays an important role in the pathogenesis but also is responsible for food contamination and spoilage. Biofilm development is often regulated by signal-mediated quorum sensing phenomenon [49]. Cells residing in biofilm are more than 1000 times more resistant to their planktonic forms. Therefore, biofilm poses a great threat to the current drug therapy. The result of biofilm biomass assay in the current investigation indicated reduced production of biofilm biomass in test pathogens when treated with OB-ZnNPs (Figure 4). Our results are agreement with previously published report of Kalishwaralal et al. [50], wherein biologically synthesized Ag nanoparticle (NPs) showed an antibiofilm activity against *P. aeruginosa* and *S. epidermis*. In an another study, Al-Shabib et al. [24]

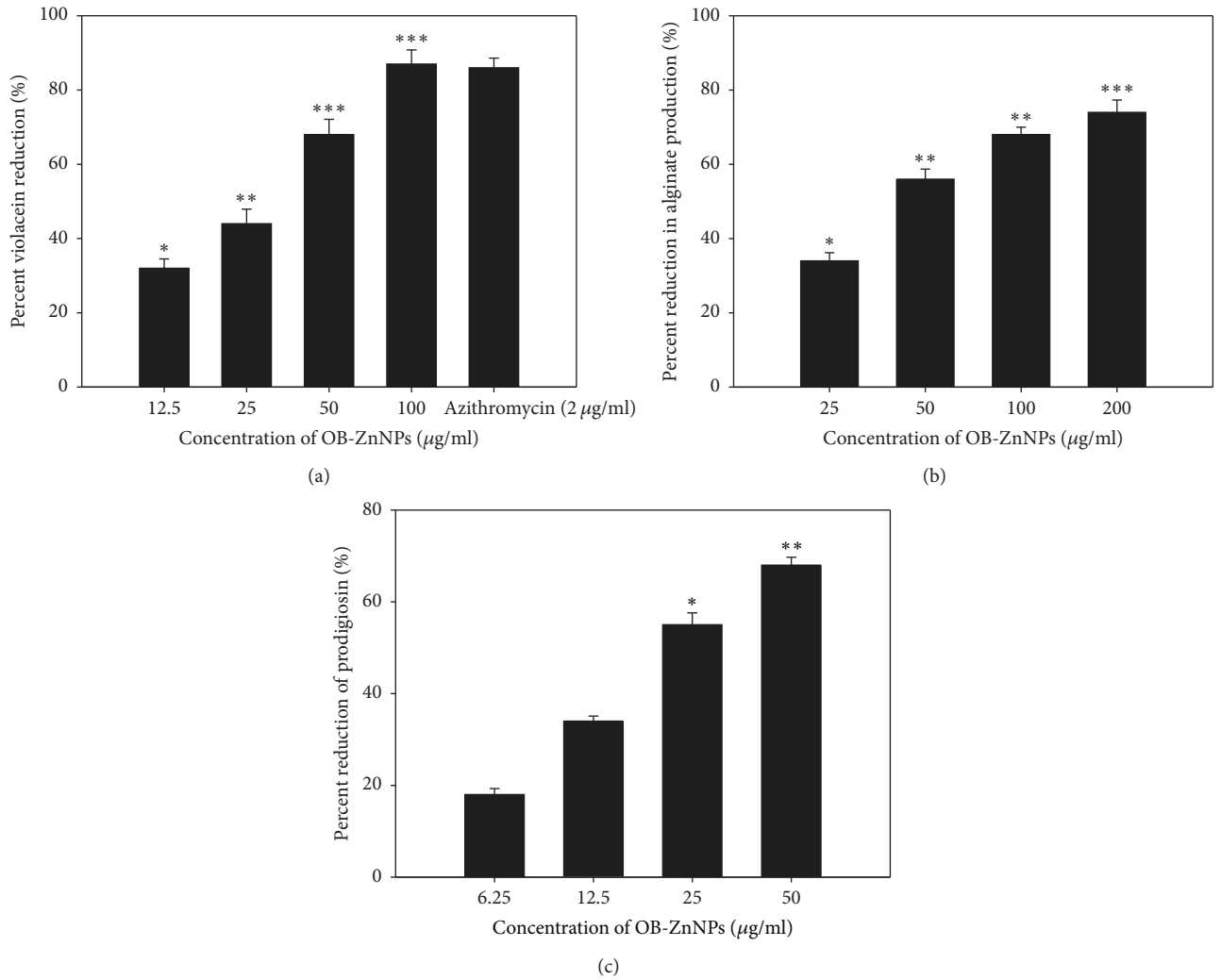

Figure 3: *Quantitative assessment of virulence factors in test pathogens at sub-MICs*. (a) Violacein inhibition in CV12472 by sub-MICs of OB-ZnNPs; (b) reduction in alginate production in *P. aeruginosa* PAO1; (c) reduction in prodigiosin production in *S. marcescens*. Data are represented as percentage of inhibition. All of the data are presented as mean ± SD. *Significance at $p \leq 0.05$; **significance at $p \leq 0.005$; ***significance at $p \leq 0.001$.

demonstrated broad-spectrum biofilm inhibition in *P. aeruginosa* PAO1, *E. coli* 25922, *L. monocytogenes*, and *C. violaceum* 12472 after treatment with sublethal doses of zinc nanostructures synthesized from the seed extract of *Nigella sativa*.

3.11. Inhibition of EPS and Swarming Motility. Exopolysaccharides (EPS) maintain biofilm architecture and microcolony formation [51]. In addition, EPS acts as a protective barrier and confers resistance to pathogens by preventing the entry of antibiotics into bacterial cells [52]. Further, increased EPS secretion means increased resistance to antimicrobials due to altered biofilm architecture [53]. Hence, inhibition of EPS production will expose biofilms cells and thus help in the eradication of biofilm. Owing to this positive correlation between biofilm formation and EPS production, an attempt was made to assess the effect of OB-ZnNPs on EPS production by test pathogens. EPS extracted from OB-ZnNPs treated and untreated cultures of test pathogens was spectrometrically analysed. EPS production in all pathogens decreased with increasing concentration of OB-ZnNPs (Figure 5(a)). OB-ZnNPs at highest sub-MICs of 200, 50, 100, 200, and 50 μg/ml exhibited 81, 69, 67, 59, and 68% decrease in EPS production in *P. aeruginosa* PAO1, *E. coli, L. monocytogenes, K. pneumoniae*, and *S. marcescens*, respectively. At lower concentrations also, significant reduction in EPS production was recorded for all pathogens (Figure 5(a)). Hsueh et al. [54] have observed 92% reduced production of EPS by *P. aeruginosa* upon treatment with 100 ng/ml concentration of copper oxide nanoparticles. LewisOscar et al. [55] also reported significant reduction of EPS produced by zinc oxide nanoparticle treated *Bacillus subtilis* strains.

Swarming motility of bacteria is also considered to be an important virulence factor, as it helps to initiate the attachment of bacterial cells to the surface [56]. Therefore, any interference with the swarming motility is bound to effect

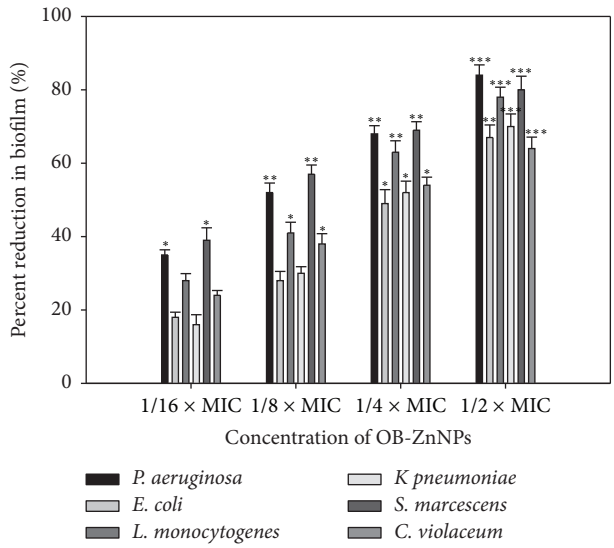

Figure 4: Quantitative measurement of biofilm inhibition as quantified by crystal violet staining. Data are represented as percentage of biofilm inhibition. All of the data are presented as mean ± SD. *Significance at $p \leq 0.05$; **significance at $p \leq 0.005$; ***significance at $p \leq 0.001$.

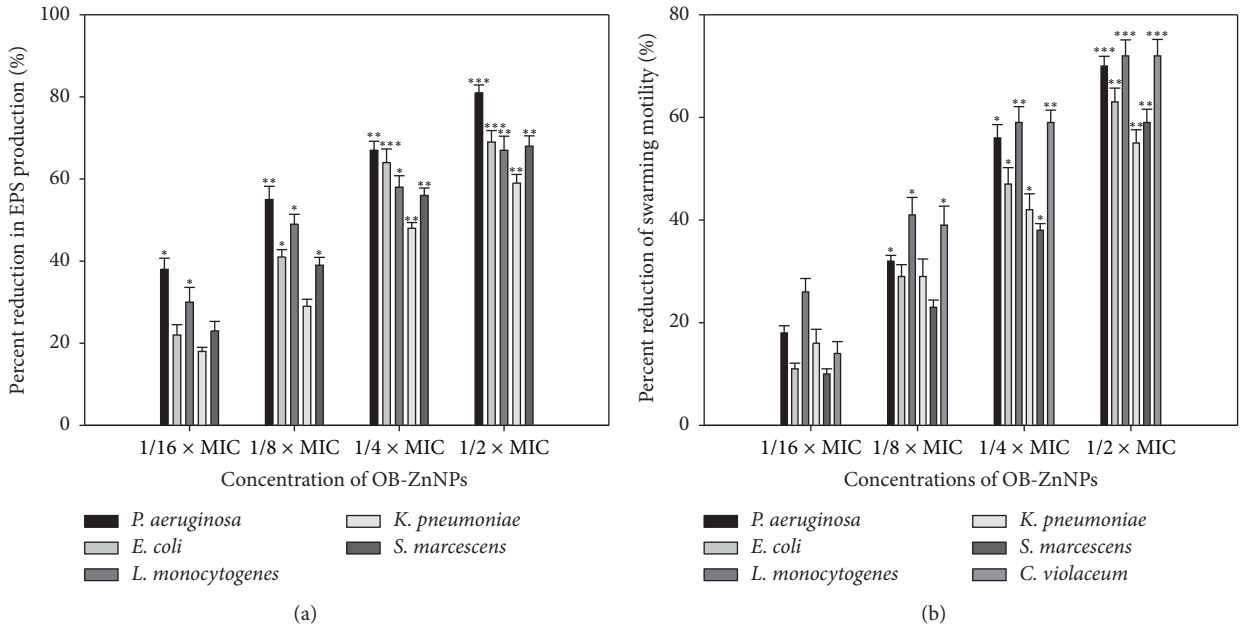

Figure 5: (a) Quantitative analysis of EPS inhibition by sub-MICs of OB-ZnNPs. (b) Inhibition of swarming motility of bacterial pathogens. Data are represented as percentage of inhibition over untreated control. All of the data are presented as mean ± SD. *Significance at $p \leq 0.05$; **significance at $p \leq 0.005$; ***significance at $p \leq 0.001$.

the biofilm formation. The OB-ZnNPs induced reduction in swarming migration of *P. aeruginosa*, *E. coli*, *L. monocytogenes, K. pneumonia*, *S. marcescens*, and *C. violaceum* is shown in Figure 5(b). The test pathogens, *P. aeruginosa*, *E. coli*, *L. monocytogenes, K. pneumonia*, *S. marcescens*, and *C. violaceum* demonstrated 18–70%, 11–63%, 26–72%, 16–55%, 10–59%, and 14–72% reduction in swarming migration in presence of sub-MICs (1/16 × MIC-1/2 × MIC) of OB-ZnNPs (Figure S1). Results obtained in the present study are comparable to the decrease in swarming motility reported in recent studies for mycofabricated silver nanoparticles [46], Ag nanoparticles synthesized from *Sargassum polyphyllum* [57], and green zinc oxide nanostructures [24].

3.12. HSA Binding Studies. The quenching in Trp fluorescence of HSA has been widely used to determine the mechanism by which a ligand interacts with HSA. In the present study, a progressive decrease in the fluorescence intensity (85%) of HSA upon NP binding was observed. The results suggested a perturbation in the microenvironment of Trp-214 which became less hydrophobic due to the binding of NP (Figure 6(a)).

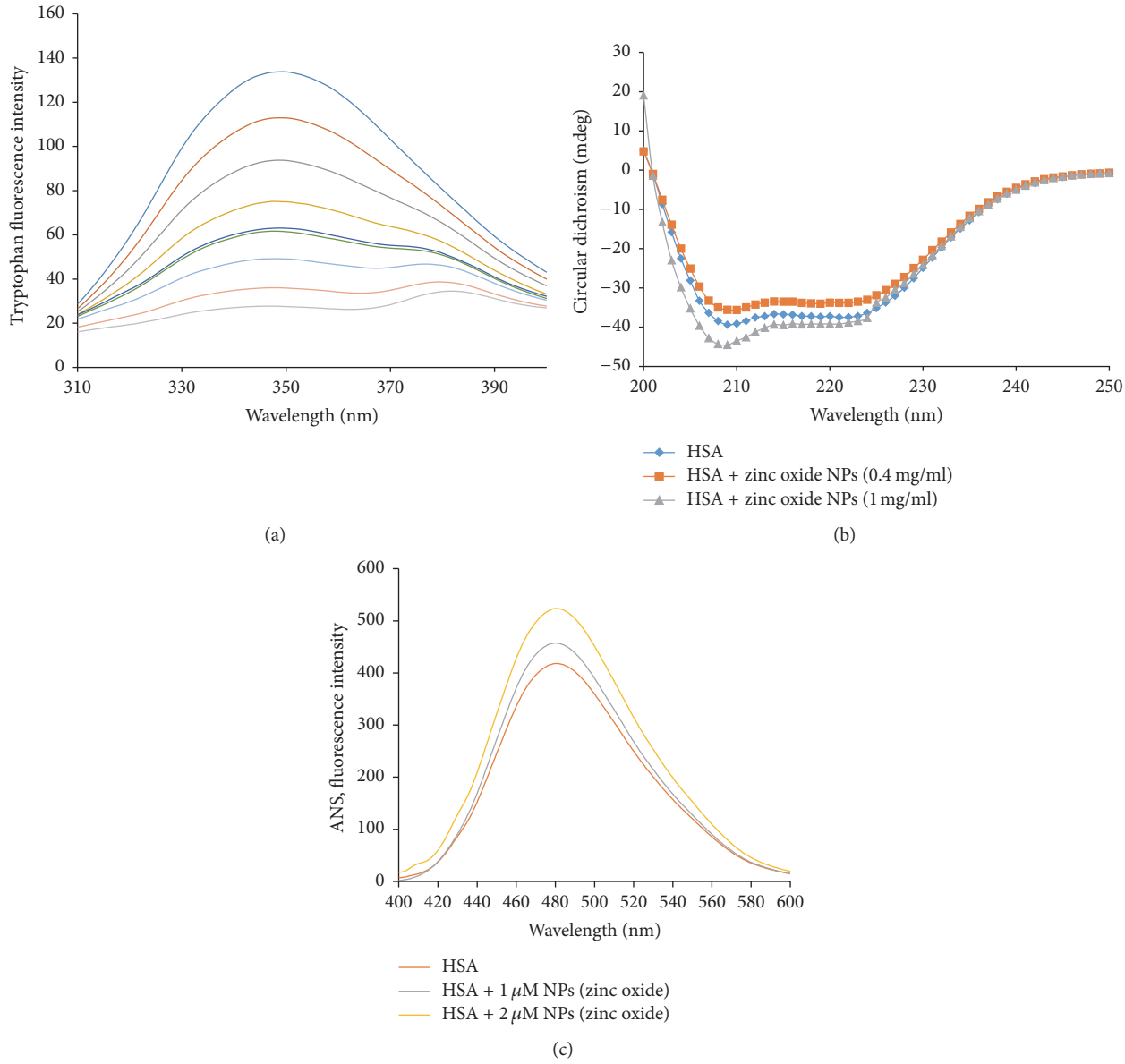

Figure 6: *Binding studies of OB-ZnNPs with human serum albumin protein*. (a) Tryptophan fluorescence analysis; (b) stability of HSA in the presence of NPs: circular dichroism analysis; (c) hydrophobicity measurement.

A change in far UV-CD spectra is generally followed to monitor any change in the secondary structure of the proteins. The far-UV spectra of HSA in the absence of OB-ZnNPs showed characteristic negative bands at 208 nm and 222 nm. Upon binding at 0.4 mg/ml concentration, a marginal decrease in the far-UV CD spectra of HSA was observed, suggesting a partial loss in the secondary structure of HSA. However, as the concentration of NP was increased to 1 mg/ml, the overall secondary structure of HSA also increased, thereby indicating a gain in the stability of the protein (Figure 6(b)). The imparted stability of the protein might be due to preferential exclusion of NPs from the surface of HSA. The results clearly suggested that the stability of secondary structure of HSA in the presence of OB-ZnNPs is concentration-dependent.

ANS dye is commonly used to map the hydrophobic patches of a protein exposed to the solvent. The results indicate that OB-ZnNPs binding to HSA induced a marginal decrease in the overall hydrophobicity of the protein (Figure 6(c)). These results are in good agreement with the results of Trp fluorescence which suggested that the microenvironment of Trp-214 became less hydrophobic upon NP binding.

3.13. *In Vivo Toxicity Studies*

3.13.1. Effect on Liver Function Tests (LFT). SGOT and SGPT are chief markers for toxic burden on liver. In the present study, SGOT was found elevated by 119.42% in the positive control (CCl4 treated animals) as compared to the control. However, OB-ZnNPs and OB-ZnNPs' groups showed

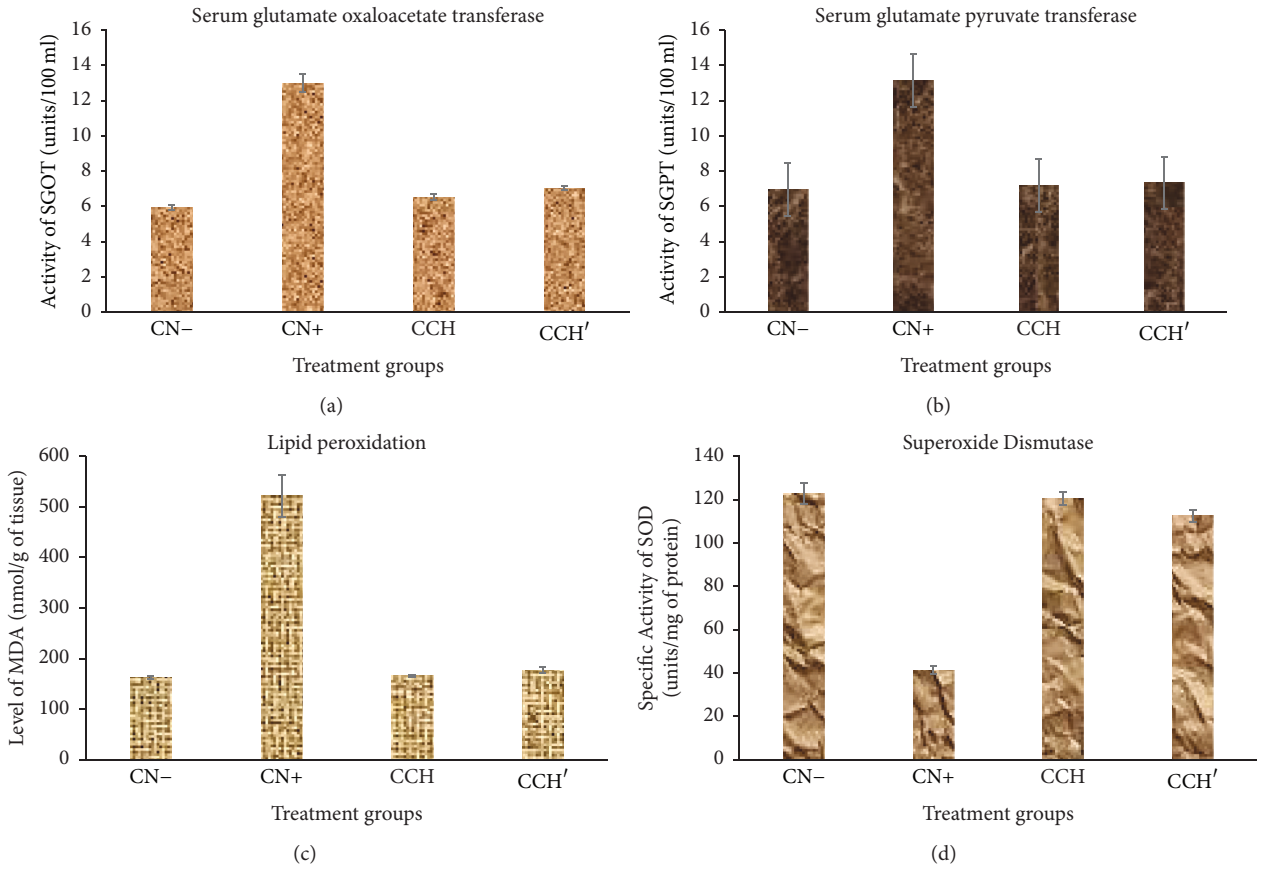

Figure 7: *In vivo* toxicity studies with OB-ZnNPs. (a, b) Effect on liver function tests (LFT), serum glutamate pyruvate transferase (SGPT), and serum glutamate oxaloacetate transferase (GOT) assay; (c) effect on MDA levels; (d) effect on antioxidant parameters.

increase in its activity by 10.14% and 18.91% with respect to the control (Figure 7(a)).

SGPT activity enhanced in CN+ by 89.46% while it increased in OB-ZnNPs and OB-ZnNPs' groups by 3.32% and 5.62% and this is statistically insignificant as compared to the control (Figure 7(b)).

3.13.2. Effect on MDA Levels. The CN+ group demonstrated elevation in MDA level by staggering 221.35% while OB-ZnNPs and OB-ZnNPs' showed merely 2.2% and 9.15% increase as compared to the control, CN−, group (Figure 7(c)).

3.13.3. Effect on Antioxidant Parameters. In the present study, SOD and GSH were chosen as antioxidant markers to assess stress level in the animals after the treatment with test nanoparticles. The CN+ group showed compromise by 66.35% and 64.34% in the activity of SOD and the level of GSH, respectively. OB-ZnNPs and OB-ZnNPs' groups exhibited decrease in SOD activity by 1.80% and 8.30% while GSH levels declined by 7.60% and 15.12% as compared to the control. This reduction was found to be statistically insignificant (Figure 7(d)).

In the present study, we were interested to know if the newly synthesized zinc oxide nanoparticles pose any toxic insults *in vivo* or to check its suitability for usage as drug or drug adjuvant. For this we chose CCl_4 as positive control which is an established hepatotoxicant in many previous investigations [58, 59]. From the *in vivo* results, it is evident that CCl4 caused severe toxicity in the parameters to assess liver health status based on significantly enhanced LFTs and MDA level concomitant with highly compromised activity of SOD and GSH. As compared to CCl4, both experimental groups, OB-ZnNPs and OB-ZnNPs', showed minor toxicity *in vivo* (Figure S2).

LFTs and MDA levels in the OB-ZnNPs and OB-ZnNPs' groups were slightly elevated while GSH level and SOD activity were quite comparable to the control (CN−). However, the minor toxicity was observed in OB-ZnNPs' group as the dose of nanoparticles was higher than that in OB-ZnNPs group. Interestingly, OB-ZnNPs group showed all the toxicity assessing parameters quite comparable to CN−. It entails that the dose of 2 mg/kg of the nanoparticles is well tolerated in the rodent system. It also suggests that the particles at this dose can be used as adjuvant with established or new drugs.

It is well established that zinc is an important trace element for all biological systems as it is involved in various biochemical and metabolic functions including copper zinc superoxide dismutase, digestion and absorption of food, hormonal homeostasis, immunity, general growth, and development [40, 60]. In the present work, it seems that the green synthesized nanoparticles improve SOD activity and assist in

absorption and digestion of the food in the treated animals. That might also improve the GSH level. Our study is well supported by earlier work done by Choi et al. [61] who showed that the zinc nanoparticles are quite tolerable at higher doses in animals. These particles hence possessed no serious toxic effect at the dose 2 mg/kg and can be used in further animal model studies for the improvement of established drugs. However, further studies are required to know the exact mechanism of action of these particles.

The findings of the current investigation highlight the broad-spectrum antibiofilm and antivirulence properties of synthesized OB-ZnNPs against human and food-borne bacterial pathogens. Efficient binding with HSA protein without changing the structure and stability augurs well for future use. Moreover, the nontoxic nature of these biofilm inhibiting nanoparticles present a possibility for use as potential nanomaterials to combat drug resistant bacterial infections and prevent contamination/spoilage of food. Exact molecular mechanism of action for these nanoparticles still needs to be unearthed.

Conflicts of Interest

The authors declare that they have no conflicts of interest.

Authors' Contributions

Nasser A. Al-Shabib and Fohad Mabood Husain contributed equally to this work.

Acknowledgments

The authors wish to acknowledge the Agricultural Research Centre, College of Food and Agricultural Sciences, and the Deanship of Scientific Research, King Saud University, Riyadh, Saudi Arabia, for funding this research.

Supplementary Materials

Supplementary material for this article includes figures for swarming motility inhibition and histopathology studies. Following is the description of the figures, FIGURE S1: effect of OB-ZnNPs on swarming motility of food pathogens. (A–F) Untreated strains and (e–h) OB-ZnNPs treated (1/2 × MIC) plates of *C. violaceum*, *E. coli*, *L. monocytogenes*, *P. aeruginosa*, *K. pneumoniae*, and *S. marcescens*, respectively. FIGURE S2: histopathological slides of various groups. A: control showing normal microstructures of the liver with well-maintained contour, hepatocytes with normal sinusoids. B: CCl_4 treated group showing disturbed microanatomy of the liver including blurred cells with prominent cytoplasmic vacuolation. Enlargement of the cells is indicative of the necrosis. C and D: representative images of liver after dose-dependent treatment with OB-ZnNPs. Both show comparable microanatomy to the control. Slight distortion is observed in image D that might be due to the usage of higher dose of nanoparticles. *(Supplementary Materials)*

References

[1] J. W. Costerton, K. J. Cheng, G. G. Geesey et al., "Bacterial biofilms in nature and disease," *Annual Review of Microbiology*, vol. 41, pp. 435–464, 1987.

[2] L. Hall-Stoodley, J. W. Costerton, and P. Stoodley, "Bacterial biofilms: from the natural environment to infectious diseases," *Nature Reviews Microbiology*, vol. 2, no. 2, pp. 95–108, 2004.

[3] R. L. E. Castrillón, R. A. Palma, and D. M. C. Padilla, "Interferencia de las biopelículasen el proceso de curación de heridas," *Dermatología Rev Mex*, vol. 55, pp. 127–139, 2011.

[4] R. M. Donlan and J. W. Costerton, "Biofilms: survival mechanisms of clinically relevant microorganisms," *Clinical Microbiology Reviews*, vol. 15, no. 2, pp. 167–193, 2002.

[5] H.-C. Flemming and H. Ridgway, "Biofilm control: conventional and alternative approaches," *Marine and Industrial Biofouling*, vol. 4, pp. 103–117, 2009.

[6] M. N. Shikongo-Nambabi, A. Shoolongela, and M. Schneider, "Control of bacterial contamination during marine fish processing," *Journal of Biology and Life Science*, vol. 3, no. 1, pp. 1–17, 2011.

[7] R. A. N. Chmielewski and J. F. Frank, "Inactivation of *Listeria monocytogenes* biofilms using chemical sanitizers and heat," in *Biofilms in The Food Environment*, H. P. Blaschek, H. H. Wang, and M. E. Agle, Eds., pp. 73–104, Blackwell Publishing, Ames, Iowa, USA, 2007.

[8] J. Harvey, K. P. Keenan, and A. Gilmour, "Assessing biofilm formation by *Listeria monocytogenes* strains," *Food Microbiology*, vol. 24, no. 4, pp. 380–392, 2007.

[9] J. N. Sofos and I. Geornaras, "Overview of current meat hygiene and safety risks and summary of recent studies on biofilms, and control of *Escherichia coli* O157:H7 in nonintact, and *Listeria monocytogenes* in ready-to-eat, meat products," *Meat Science*, vol. 86, no. 1, pp. 2–14, 2010.

[10] U. Desselberger, "Emerging and re-emerging infectious diseases," *Infection*, vol. 40, no. 1, pp. 3–15, 2000.

[11] R. P. Allaker, "The use of nanoparticles to control oral biofilm formation," *Journal of Dental Research*, vol. 89, no. 11, pp. 1175–1186, 2010.

[12] J. R. Morones, J. L. Elechiguerra, A. Camacho et al., "The bactericidal effect of silver nanoparticles," *Nanotechnology*, vol. 16, no. 10, pp. 2346–2353, 2005.

[13] J. Sawai, "Quantitative evaluation of antibacterial activities of metallic oxide powders (ZnO, MgO and CaO) by conductimetric assay," *Journal of Microbiological Methods*, vol. 54, no. 2, pp. 177–182, 2003.

[14] I. Sondi and B. Salopek-Sondi, "Silver nanoparticles as antimicrobial agent: a case study on *E. coli* as a model for gram-negative bacteria," *Journal of Colloid and Interface Science*, vol. 275, no. 1, pp. 177–182, 2004.

[15] R. Brayner, R. Ferrari-Iliou, N. Brivois, S. Djediat, M. F. Benedetti, and F. Fievet, "Toxicological impact studies based on *Escherichia coli* bacteria in ultrafine ZnO nanoparticles colloidal medium," *Nano Letters*, vol. 6, no. 4, pp. 866–870, 2006.

[16] O. Yamamoto, "Influence of particle size on the antibacterial activity of zinc oxide," *International Journal of Inorganic Materials*, vol. 3, no. 7, pp. 643–646, 2001.

[17] E. Casals, T. Pfaller, A. Duschl, G. J. Oostingh, and V. Puntes, "Time evolution of the nanoparticle protein corona," *ACS Nano*, vol. 4, no. 7, pp. 3623–3632, 2010.

[18] S. Laera, G. Ceccone, F. Rossi et al., "Measuring protein structure and stability of protein-nanoparticle systems with synchrotron radiation circular dichroism," *Nano Letters*, vol. 11, no. 10, pp. 4480–4484, 2011.

[19] W. Shang, J. H. Nuffer, J. S. Dordick, and R. W. Siegel, "Unfolding of ribonuclease a on silica nanoparticle surfaces," *Nano Letters*, vol. 7, no. 7, pp. 1991–1995, 2007.

[20] V. Kumar and S. K. Yadav, "Plant-mediated synthesis of silver and gold nanoparticles and their applications," *Journal of Chemical Technology and Biotechnology*, vol. 84, no. 2, pp. 151–157, 2009.

[21] K. Jeeva, M. Thiyagarajan, V. Elangovan, N. Geetha, and P. Venkatachalam, "*Caesalpinia coriaria* leaf extracts mediated biosynthesis of metallic silver nanoparticles and their antibacterial activity against clinically isolated pathogens," *Industrial Crops and Products*, vol. 52, pp. 714–720, 2014.

[22] G. Sangeetha, S. Rajeshwari, and R. Venckatesh, "Green synthesis of zinc oxide nanoparticles by *aloe barbadensis miller* leaf extract: structure and optical properties," *Materials Research Bulletin*, vol. 46, no. 12, pp. 2560–2566, 2011.

[23] M. Sundrarajan, S. Ambika, and K. Bharathi, "Plant-extract mediated synthesis of ZnO nanoparticles using *Pongamia pinnata* and their activity against pathogenic bacteria," *Advanced Powder Technology*, vol. 26, no. 5, pp. 1294–1299, 2015.

[24] N. A. Al-Shabib, F. M. Husain, F. Ahmed et al., "Biogenic synthesis of Zinc oxide nanostructures from *Nigella sativa* seed: prospective role as food packaging material inhibiting broad-spectrum quorum sensing and biofilm," *Scientific Reports*, vol. 6, article 36761, 2016.

[25] F. A. Qurainy, M. Nadeem, S. Khan, S. Alansi, and M. Tarroum, "Efficient regeneration of a potential medicinal plant *Ochradenus baccatus* delile from cotyledon and shoot axis," *Pakistan Journal of Botany*, vol. 45, no. 2, pp. 501–505, 2013.

[26] A. Hassan-Abdallah, A. Merito, S. Hassan et al., "Medicinal plants and their uses by the people in the Region of Randa, Djibouti," *Journal of Ethnopharmacology*, vol. 148, no. 2, pp. 701–713, 2013.

[27] A. L. Patterson, "The scherrer formula for X-ray particle size determination," *Physical Review A: Atomic, Molecular and Optical Physics*, vol. 56, no. 10, pp. 978–982, 1939.

[28] CLSI, *Performance Standards for Antimicrobial Susceptibility Testing: Seventeenth Informational Supplement: M100-S17*, Clinical and Laboratory Standards Institute, Wayne, Pa, USA, 2007.

[29] R. S. Blosser and K. M. Gray, "Extraction of violacein from *Chromobacterium violaceum* provides a new quantitative bioassay for N-acyl-homoserine lactone autoiducers," *Journal of Microbiological Methods*, vol. 40, no. 1, pp. 47–55, 2000.

[30] V. Gopu, C. K. Meena, P. H. Shetty, and Y. He, "Quercetin influences quorum sensing in food borne bacteria: in-vitro and in-silico evidence," *PLoS ONE*, vol. 10, no. 8, Article ID e0134684, 2015.

[31] T. Morohoshi, T. Shiono, K. Takidouchi et al., "Inhibition of quorum sensing in *Serratia marcescens* AS-1 by synthetic analogs of N-acylhomoserine lactone," *Applied and Environmental Microbiology*, vol. 73, no. 20, pp. 6339–6344, 2007.

[32] F. M. Husain and I. Ahmad, "Doxycycline interferes with quorum sensing-mediated virulence factors and biofilm formation in Gram-negative bacteria," *World Journal of Microbiology and Biotechnology*, vol. 29, no. 6, pp. 949–957, 2013.

[33] A. L. Huston, B. Methe, and J. W. Deming, "Purification, characterization, and sequencing of an extracellular cold-active aminopeptidase produced by marine psychrophile *Colwellia psychrerythraea* strain 34H," *Applied and Environmental Microbiology*, vol. 70, no. 6, pp. 3321–3328, 2004.

[34] M. K. Dubois, J. K. Gils, P. A. Hanniton, and F. Smith, "Use of phenol reagent for the determination of total sugar," *Analytical Chemistry*, vol. 28, pp. 350–356, 1956.

[35] G. A. O'Toole and R. Kolter, "Initiation of biofilm formation in *Pseudomonas fluorescens* WCS365 proceeds via multiple, convergent signalling pathways: a genetic analysis," *Molecular Microbiology*, vol. 28, no. 3, pp. 449–461, 1998.

[36] R. Wahab, S. Dwivedi, M. S. Khan et al., "Optical analysis of zinc oxide quantum dots with bovine serum albumin and bovine hemoglobin," *Journal of Pharmaceutical Innovation*, vol. 9, no. 1, pp. 48–52, 2014.

[37] M. T. Rehman, S. Ahmed, and A. U. Khan, "Interaction of meropenem with 'N' and 'B' isoforms of human serum albumin: a spectroscopic and molecular docking study," *Journal of Biomolecular Structure and Dynamics*, vol. 34, no. 9, pp. 1849–1864, 2016.

[38] M. T. Rehman, H. Shamsi, and A. U. Khan, "Insight into the binding mechanism of imipenem to human serum albumin by spectroscopic and computational approaches," *Molecular Pharmaceutics*, vol. 11, no. 6, pp. 1785–1797, 2014.

[39] R. P. Honda, K.-I. Yamaguchi, and K. Kuwata, "Acid-induced molten globule state of a prion protein:Crucial role of strand 1-Helix 1-Strand 2 Segment," *The Journal of Biological Chemistry*, vol. 289, no. 44, pp. 30355–30363, 2014.

[40] H. Ebaid, J. Al-Tamimi, I. Hassan, I. Alhazza, and M. Al-Khalifa, "Antioxidant bioactivity of samsum Ant (Pachycondyla sennaarensis) Venom protects against CCL_4-induced nephrotoxicity in mice," *Oxidative Medicine and Cellular Longevity*, vol. 2014, Article ID 763061, 2014.

[41] S. Marklund and G. Marklund, "Involvement of the superoxide anion radical in the autoxidation of pyrogallol and a convenient assay for superoxide dismutase," *European Journal of Biochemistry*, vol. 47, no. 3, pp. 469–474, 1974.

[42] D. J. Jollow, J. R. Mitchell, N. Zampaglione, and J. R. Gillette, "Bromobenzene induced liver necrosis. Protective role of glutathione and evidence for 3,4 bromobenzene oxide as the hepatotoxic metabolite," *Pharmacology*, vol. 11, no. 3, pp. 151–169, 1974.

[43] J. A. Buege and S. D. Aust, "Microsomal lipid peroxidation," *Methods in Enzymology*, vol. 52, pp. 302–310, 1978.

[44] S. Nagarajan and K. Arumugam Kuppusamy, "Extracellular synthesis of zinc oxide nanoparticle using seaweeds of gulf of Mannar, India," *Journal of Nanobiotechnology*, vol. 11, no. 1, article 39, 2013.

[45] M. S. Wagh, R. H. Patil, D. K. Thombre, M. V. Kulkarni, W. N. Gade, and B. B. Kale, "Evaluation of anti-quorum sensing activity of silver nanowires," *Applied Microbiology and Biotechnology*, vol. 97, no. 8, pp. 3593–3601, 2013.

[46] B. R. Singh, B. N. Singh, A. Singh, W. Khan, A. H. Naqvi, and H. B. Singh, "Mycofabricated biosilver nanoparticles interrupt *Pseudomonas aeruginosa* quorum sensing systems," *Scientific Reports*, vol. 5, Article ID 13719, 2015.

[47] I. A. S. V. Packiavathy, S. Priya, S. K. Pandian, and A. V. Ravi, "Inhibition of biofilm development of uropathogens by curcumin - An anti-quorum sensing agent from *Curcuma longa*," *Food Chemistry*, vol. 148, pp. 453–460, 2014.

[48] C. Nithya, C. Aravindraja, and S. K. Pandian, "*Bacillus pumilus* of Palk Bay origin inhibits quorum-sensing-mediated virulence

factors in Gram-negative bacteria," *Research in Microbiology*, vol. 161, no. 4, pp. 293–304, 2010.

[49] B. V. Jones, R. Young, E. Mahenthiralingam, and D. J. Stickler, "Ultrastructure of *Proteus mirabilis* swarmer cell rafts and role of swarming in catheter-associated urinary tract infection," *Infection and Immunity*, vol. 72, no. 7, pp. 3941–3950, 2004.

[50] K. Kalishwaralal, S. BarathManiKanth, S. R. K. Pandian, V. Deepak, and S. Gurunathan, "Silver nanoparticles impede the biofilm formation by *Pseudomonas aeruginosa* and *Staphylococcus epidermidis*," *Colloids and Surfaces B: Biointerfaces*, vol. 79, no. 2, pp. 340–344, 2010.

[51] K. Sauer and A. K. Camper, "Characterization of phenotypic changes in *Pseudomonas putida* in response to surface-associated growth," *Journal of Bacteriology*, vol. 183, no. 22, pp. 6579–6589, 2001.

[52] C. A. Fux, J. W. Costerton, P. S. Stewart, and P. Stoodley, "Survival strategies of infectious biofilms," *Trends in Microbiology*, vol. 13, no. 1, pp. 34–40, 2005.

[53] F. H. Yildiz and G. K. Schoolnik, "Vibrio cholerae O1 El Tor: identification of a gene cluster required for the rugose colony type, exopolysaccharide production, chlorine resistance, and biofilm formation," *Proceedings of the National Acadamy of Sciences of the United States of America*, vol. 96, no. 7, pp. 4028–4033, 1999.

[54] Y. Hsueh, W. Ke, C. Hsieh et al., "ZnO nanoparticles affect *Bacillus subtilis* cell growth and biofilm formation," *PLoS ONE*, vol. 10, no. 6, Article ID e0128457, 2015.

[55] F. LewisOscar, D. MubarakAli, C. Nithya et al., "One pot synthesis and anti-biofilm potential of copper nanoparticles (CuNPs) against clinical strains of *Pseudomonas aeruginosa*," *Biofouling*, vol. 31, no. 4, pp. 379–391, 2015.

[56] L. A. Pratt and R. Kolter, "Genetic analysis of *Escherichia coli* biofilm formation: roles of flagella, motility, chemotaxis and type I pili," *Molecular Microbiology*, vol. 30, no. 2, pp. 285–293, 1998.

[57] M. Arunkumar, K. Suhashini, N. Mahesh, and R. Ravikumar, "Quorum quenching and antibacterial activity of silver nanoparticles synthesized from *Sargassum polyphyllum*," *Bangladesh Journal of Pharmacology*, vol. 9, no. 1, pp. 54–59, 2014.

[58] M. Boll, L. W. D. Weber, E. Becker, and A. Stampfl, "Mechanism of carbon tetrachloride-induced hepatotoxicity. Hepatocellular damage by reactive carbon tetrachloride metabolites," *Zeitschrift fur Naturforschung - Section C Journal of Biosciences*, vol. 56, no. 7-8, pp. 649–659, 2001.

[59] H. Ebaid, I. Hassan, S. Bashandy et al., "Zinc improves the immune function and the proliferation of lymphocytes in Cadmium-treated rats," *Central European Journal of Immunology*, vol. 39, no. 4, pp. 441–448, 2014.

[60] A. Malhotra and D. K. Dhawan, "Current view of zinc as a hepatoprotective agent in conditions of chlorpyrifos induced toxicity," *Pesticide Biochemistry and Physiology*, vol. 112, no. 1, pp. 1–6, 2014.

[61] J. Choi, H. Kim, P. Kim et al., "Toxicity of zinc oxide nanoparticles in rats treated by two different routes: single intravenous injection and single oral administration," *Journal of Toxicology and Environmental Health, Part A. Current Issues*, vol. 78, no. 4, pp. 226–243, 2015.